Journal of Molecular Liquids 341 (2021) 117309

Contents lists available at ScienceDirect

Journal of Molecular Liquids

journal homepage: www.elsevier.com/locate/molliq

Role of ionic surfactants on the nucleation and growth of silver nanoparticles

Haya Alsubaie, Zoya Zaheer *, Elham Shafik Aazam

Department of Chemistry, Faculty of Science, P.O. Box 80203, King Abdulaziz University, Jeddah 21589, Saudi Arabia

ARTICLE INFO

Article history:
Received 23 May 2021
Revised 3 August 2021
Accepted 16 August 2021
Available online 20 August 2021

Keywords:
Nucleation
Raman spectra
Kinetics
Surfactant
Silver nanoparticles

ABSTRACT

Sodium dodecyl sulfate (SDS) and cetyltrimethylammonium bromide (CTAB) were used as stabilizers for the preparation of silver nanoparticles (AgNPs) by the reduction of silver nitrate with proanthocyanidines (Pas). UV–visible spectra shows that the surface Plasmon resonance (SPR) intensity of AgNPs increases and decreases with increasing SDS and became constant at higher concentration. CTAB has no effect on the nucleation of AgNPs due to the insolubility of Pas. The position of SPR band (λ_{max} = from 438 to 476 nm) depends on the concentration of Pas and a red shift of 38 nm was observed in absence of externally added SDS. The micellar pseudo phase proposed by Menger and Portnoy, modified by Bunton was used to determine the rate constants in micellar media. The Ag^+ ions were formed complex with negative head group (—O—SO_3^-) of SDS electrostatically. Raman scattering spectroscopy, transmission electron microscopy, and scanning electron microscopy were used to discuss the capping action of SDS. Zeta potential of SDS-capped AgNPs was negative and resulting sols were stable for many months.

1. Introduction

Due to the potential application of transition metal nanoparticles in different aspects of human life, fabrication and characterization of plasmonic advanced nanoparticles have been the interest of various investigators from many decades [1,2]. Generally, surfactant (normal and Gemini), polymer (natural and synthetic), lipids, protein, organic solvents, plants extract and ligands have been used as stabilizing agents [3–7]. Surfactants have advantageous over the other capping agent due to the formation of micelles (various aggregates) and their unique solubilization properties. For example, Bakshi and his coworkers used different surfactant as a capping agent for the synthesis of silver, gold, iron, selenium, tellurium metal nanoparticles and reported that the presence of surfactant acted as a capping agent, which be easily removed by washing from the surface of nanoparticles [1,8–10]. Transition metal nano-crystals have shown an excellent potential catalytic and adsorption activities, these depends on the size and shape. Morphology of nanoparticles strongly depends on the nature of reducing agent (strong and weak) and presence of a stabilizer [11]. The selection of stabilizer was a crucial problem for preparation of nanoparticles having desired morphology [12]. It has been established that the presence of a suitable stabilizer was essential to control the unlimited growth of NPs formation [13–15].

Silver and gold nanoparticles have a sharp well-defined localized surface Plasmon resonance band in the UV–visible region and exhibit a unique optical property due to the collective oscillation of conduction band electrons confined in the nanoparticles. Optical properties of plasmonic nanoparticles can be altering by adding additives as well as stabilizer. Multi-branched gold nanoparticles (mono-, bi-, tri-, tetra-, and multi-pods) were prepared by using CTAB [16,17], bis-(p-sulfonatophynyl)phenylpho sphine dihydrate dipotassium [18], and SDS as a stabilizing agents [19]. Bakr et al. reported the high yield synthesis of urchin-like gold nanoparticles using different sulphur containing ligands as capping agents [20]. Xaio and Qi discussed the various surfactant based strategies such as adsorbate-directed, seed-mediated, template-assisted, control of growth kinetics, single surfactant-directed, mixed surfactant-directed, super molecular surfactant-directed and metal–surfactant complex template for the preparation of gold nanoparticles in his pioneering feature article [21]. Out of these, metal–surfactant complex strategy is a simple and cost effect technique for the synthesis of advanced metal nanomaterials having different morphologies. The use of natural plants extract avoid the necessity of toxic chemicals as a stabilizing agent [22,23]. Proanthocyanidines (water soluble and condensed tannins) are the colorless polyphenolic polymeric compounds widely found in plant kingdom, exist in many food and protects the plant against predator and ultraviolet radiation [24]. They are the

* Corresponding author.
E-mail address: zzkhan@kau.edu.sa (Z. Zaheer).

https://doi.org/10.1016/j.molliq.2021.117309
0167-7322/

oligomers and polymers of flavan-3-ol units, mainly (+)-catechin, (-)-epicatechin and their derivatives [25,26]. Valls and his coworkers pointed out that the separation of Pas from the plant and food sources was complicated due to the presence of enormous isomeric oligomers by chromatographically [27].

Metal-surfactant (Ag^+-SDS) complex strategy was used for the synthesis of advanced SDS capped AgNPs for the first time. We have demonstrated the capping action of ionic surfactants on the stability of AgNPs using water soluble Rubus leaves extract as a reducing agent, which are the rich exporter of Pas, anthocyanins, and other polyphenolic antioxidants [28,29]. A series of kinetic experiments were performed in presence of anionic and cationic surfactants, namely, CTAB and SDS to establish the head groups of stabilizers on the morphology of AgNPs. Raman scattering spectroscopy was used to determine the mode of action of SDS towards AgNPs for the first time.

2. Experimental

2.1. Materials

Rebus sanctus leaves were collected from the garden of King Abdulaziz University, Jeddah. Silver nitrate ($AgNO_3$, molar

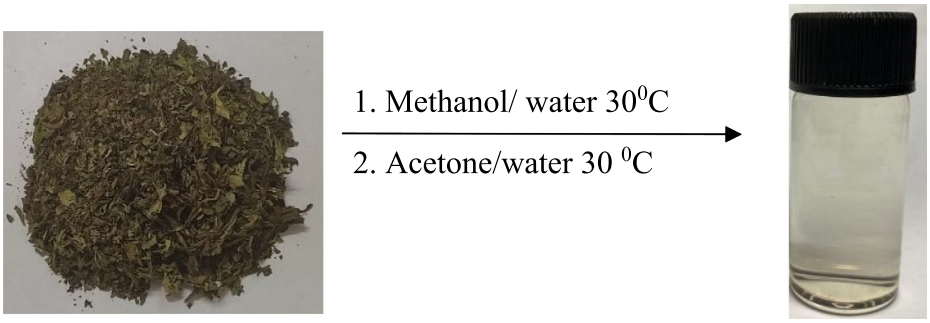

Scheme 1. Extraction of Pas from Rebus Sanctus leaves.

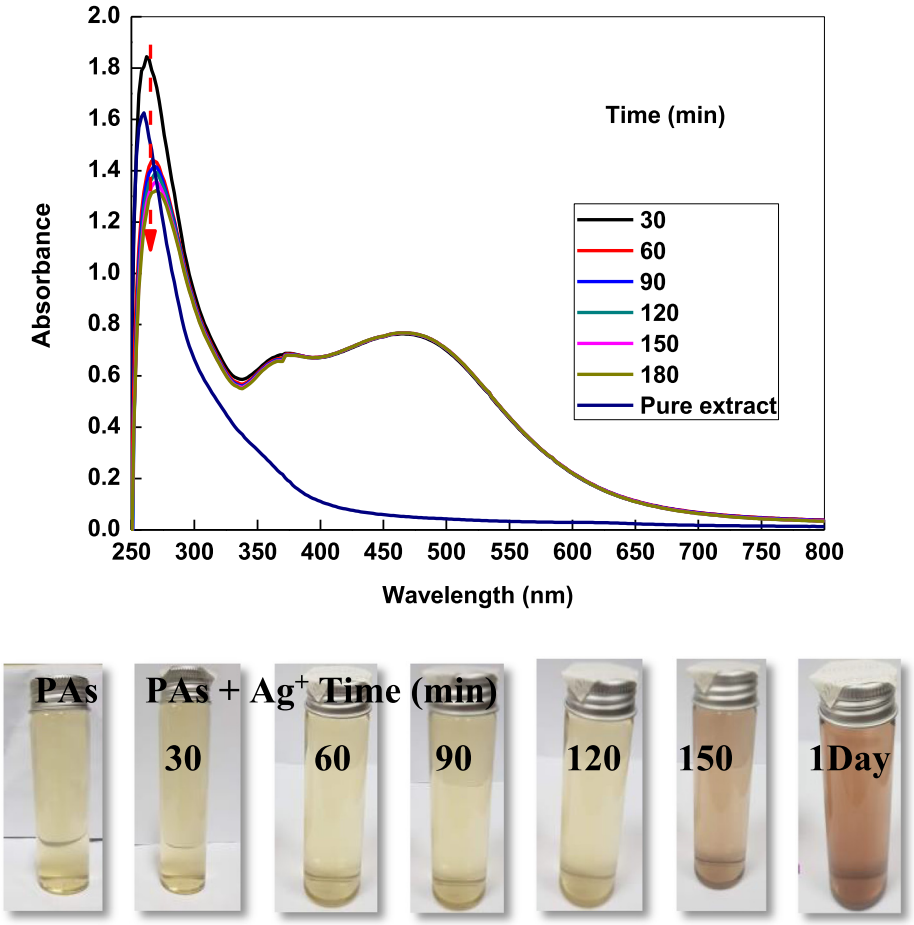

Fig. 1. UV–visible of proanthocyanidins, time-resolved UV–visible spectra and optical images of AgNPs formation at 25 °C. Reaction conditions: [$AgNO_3$] = 1.0 mM, [Pas] = 40 % (A), and 10, 30, 40% (B).

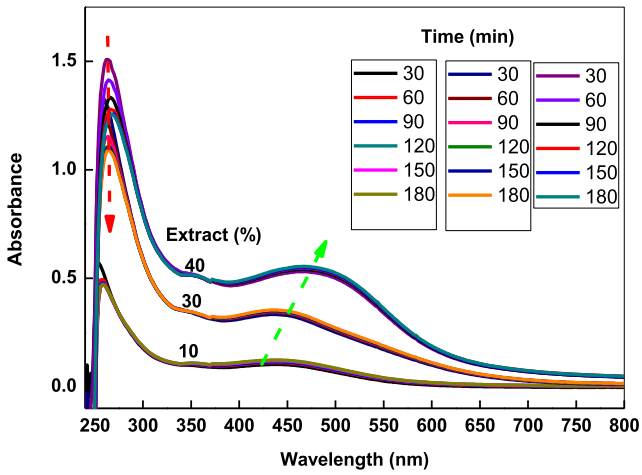

Fig. 1 (*continued*)

mass = 169.87 g/mol), cetyltrimethylammonium bromide ($C_{19}H_{42}$-NBr, molar mass = 364.45 g/mol), sodium dodecyl sulfate ($C_{12}H_{25}$-SO_4Na, molar mass = 288.372 g/mol), NaCl, NaBr and other reagents (All Sigma-Aldrich and purity ≥ 99.9%) were used as received without further purification. The stock solutions were prepared in deionized water on the molarity basis. Silver nitrate solution was kept in amber color glass container.

2.2. Preparation of extract and separation of Pas

Rebus Sanctus leaves (15 g) washed with tap water followed by distilled water, cut in small pieces and ground well into powder by milling. The 250 ml of water + acetone (70%, v/v) was taken in a conical flask and shrubs powder was added. It was stirred with magnetic stirrer for 24 h at room temperature and filtered with Whatman paper No.1. For extraction of water soluble PAs, the reported method was used with slight modification [30]. In briefly, the resulting filtrate was recovered, washed with 100 ml chloroform and separated by liquid–liquid extraction with separating funnel to remove the non-polar and lipophilic impurities. The extraction procedure was repeated for 2 times with chloroform. The water–acetone layer was again treated with 100 ml ethyl acetate for two times to remove the monomeric flavonoids and was concentrated by using rotatory evaporator at 50 °C. The 50% (v/v) methanol–water mixture was added into resulting aqueous solution and then loaded on a manually packed Sephadex LH 20-column (pre-equilibrated with 50% (v/v) methanol–water solu-

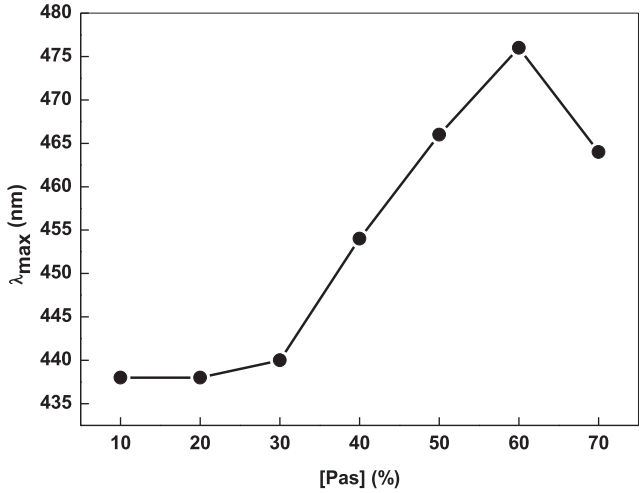

Fig. 2. Effects of Pas concentration (red shift) on the λ_{max} of silver sols.

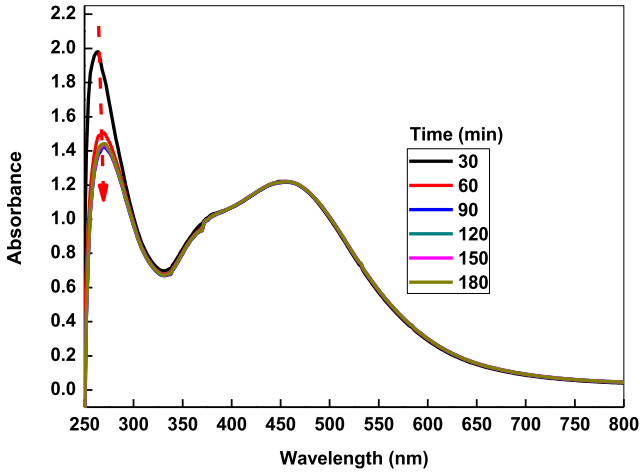

Fig. 3. Time-resolved UV–visible spectra of AgNPs formation as a function of $AgNO_3$ concentration at 25 °C. Reaction conditions: [Pas] = 50%, [$AgNO_3$] = 1.0 (A), 3.0 (B) and 4.0 mM (C).

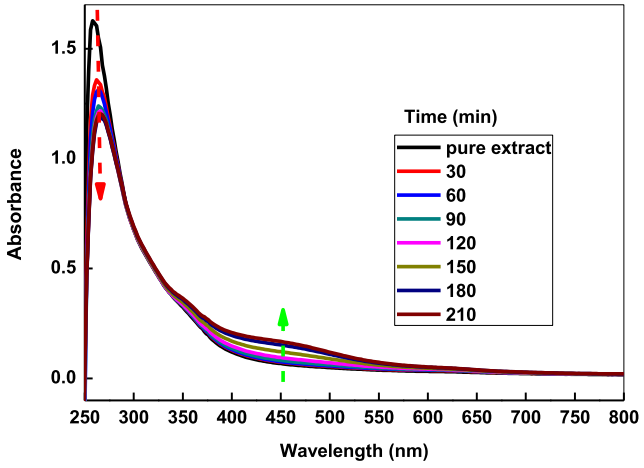

Fig. 3 (*continued*)

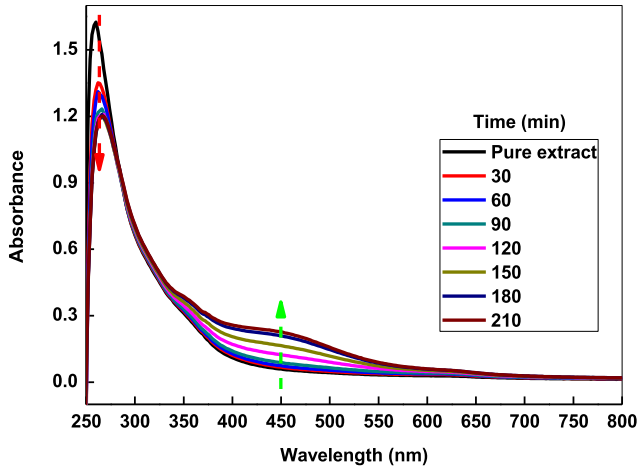

Fig. 3 (*continued*)

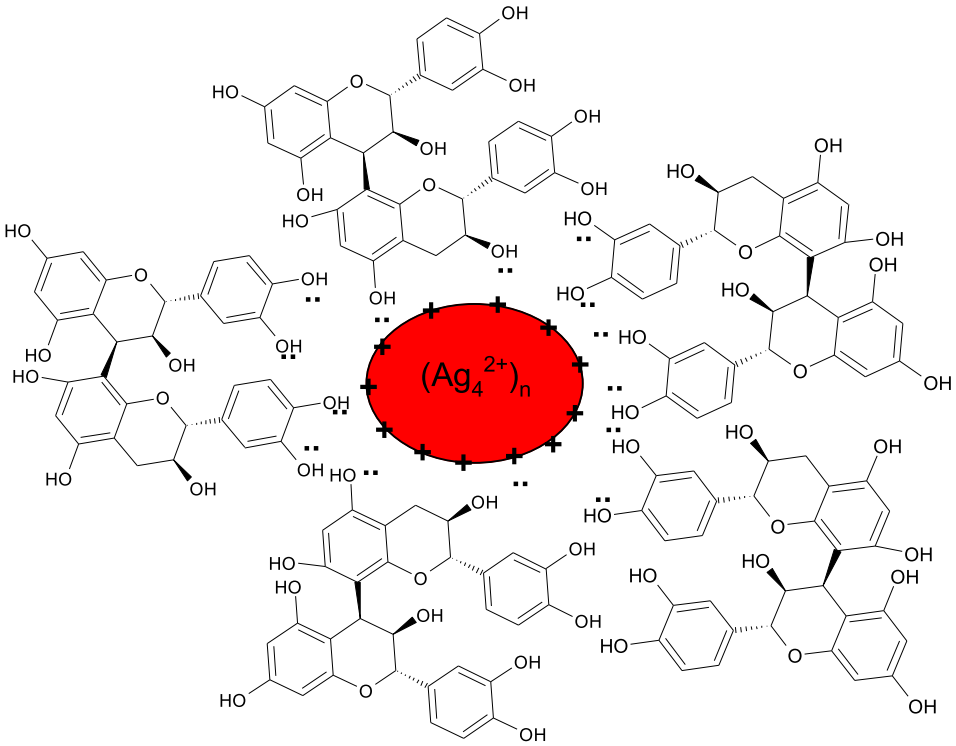

Scheme 2. Capping action of Pas towards AgNPs.

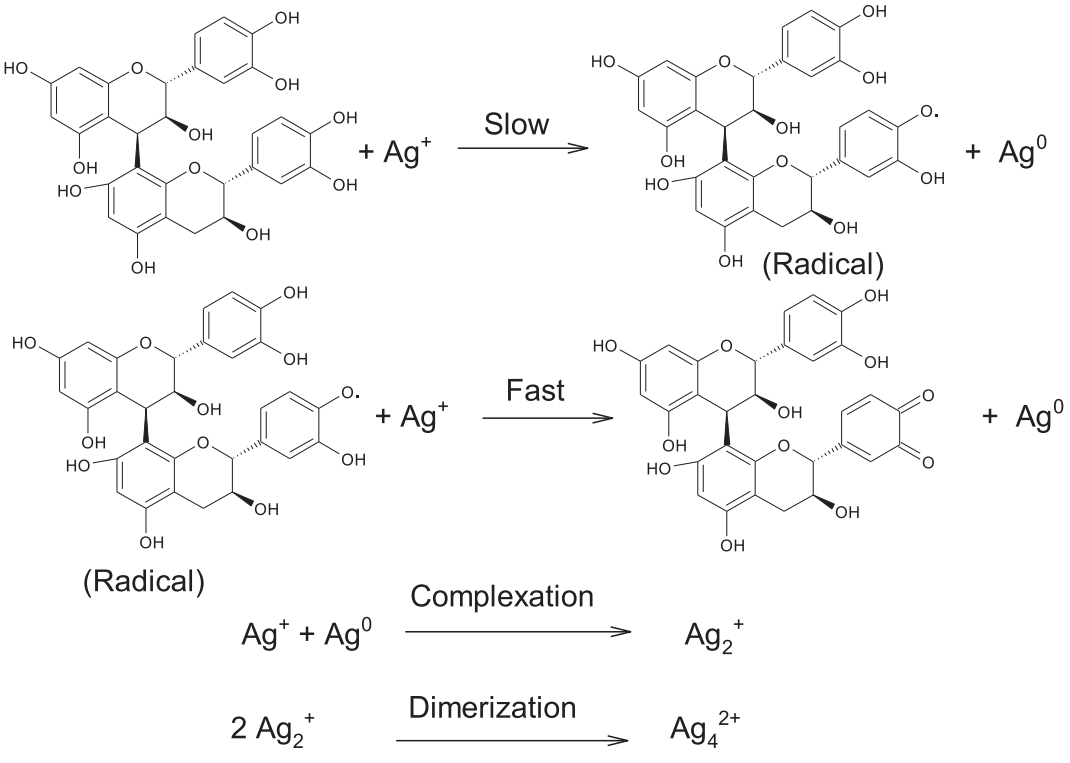

Scheme 3. Reduction of Ag^+ into metallic silver by Pas.

tion). For the removal of anthocyanins, monomeric flavonoids and reducing sugars, the column was eluted with 50% methanol–water solution [31]. The acetone–water 70% was used for the elution of Pas form the column. The acetone was removed at room temperature and resulting aqueous solution was used for the estimation of Pas by recording the UV–visible spectra from 250 to 800 nm. Most of the polyphenolic compounds show a well-defined absorption peak at 250–320 and are colorless. On the other hand, anthocyans exhibited sharp peak in the vicinity of 520 nm and produces dark red color [32]. The aqueous phase was also lyophilized to dryness

to obtain the Pas in solid form. The aqueous fraction was used as a reducing agent for the synthesis of AgNPs. Schematic extraction of Pas from Rebus Sanctus leaves are given in Scheme 1.

2.3. AgNPs preparation and characterization

To establish the reducing nature of Pas, the AgNPs were prepared at room temperature. In a typical experiment, the aqueous solution Pas (from 10% to 70%) was added in a reaction vessel containing the required amount of $AgNO_3$ (1.0 mM). The reaction mixture was stirred magnetically at room temperature. The pale, yellow, orange to red color appeared with increasing the reaction time, indicating the formation of AgNPs (reduction of Ag^+ by Pas into metallic Ag). The progress of redox-reaction was followed by measuring the UV–visible spectra of resulting silver sols in the entire UV–visible region. The same experiment was performed with CTAB and SDS to determine the stability of AgNPs. For the solid separation, the sols were centrifuged with 1500 rpm for 20 min. the solid was washed with distilled water, and dried at room temperature. UV–visible spectroscope provides preliminary information about the shape, size and the size distribution of metal NPs. Therefore, UV–visible spectra of AgNPs were recorded on A Perkin Elmer Lambda-25 UV/visible spectrophotometer equipped with 1.0 cm quartz cell. Surface morphology, composition, and capping action of stabilizers were established with using conventional spectroscopic methods such as transmission electron microscopy (TEM), scanning electron microscope (SEM), and Raman scattering spectroscopy. The TEM images were recorded by using JEOL JEM-1011, Japan, and transmission electron microscope operating at 200 kV accelerating voltage with a specimen set at an 8 mm working distance. For the Raman experiments, few drops of the SDS-Ag suspensions were deposited onto glass slides and dried in air at room temperature. We used a Labram HR800 Horiba Jobin-Yvon spectrometer with an Ar^+ laser beam excitation at 514.5 nm.

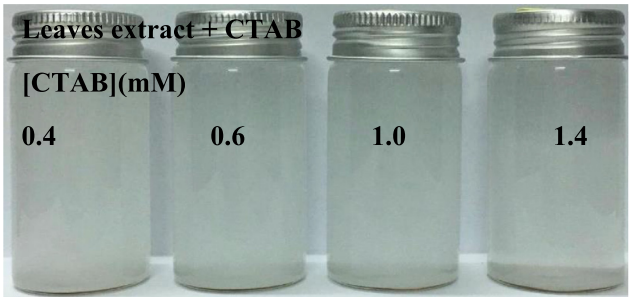

Scheme 4. Effect of CTAB on the solubility of Pas.

3. Results and discussion

3.1. General consideration

The UV–visible spectrum of Pas shows a sharp symmetrical absorption peak at 275 nm in the range of 250–300 nm and no significant absorbance beyond 300 nm (Fig. 1A; blue line), which is the spectral characteristic of catechin-like Pas ($\pi \rightarrow \pi^*$ electronic transition) isolated with aqueous acetone [33]. Lin and Harnly used ultraviolet absorbance for the quantification of standard hydrolysable tannins and reported that the position of absorption peak (λ_{max}) were remains constant for the various isomers stereoisomers of dimer standard as compared to the monomer of Pas [34]. Optical images also show that the resulting Pas exhibit pale yellow color (Fig 1.0). Flavonoids absorb light in the UV–visible spectrum between 250–290 nm and 320–385 nm due to the transition of ring A and ring B, respectively, and produces pale yellow and colorless to the human eye [35]. Ku and Mun also reported the absorption peak at 280 nm for the Pas isolated from pinus radiate bark using hot water [36]. Revilla et al. reported that the catechins and Pas show an absorption peak in the vicinity of 270–280 nm [37]. Thus we may state confidently that the Pas were the main chemical constituents of Rebus sanctus leaves extract under our experimental conditions.

3.2. Reducing nature of Pas

For the synthesis of AgNPs, Pas was used as a reducing agent. In the first set of kinetic experiments, the different amounts of Pas solutions (ranging from 10% to 70%) were added in different stoppered conical flask containing the same concentration of $AgNO_3$ (=1.0 mM) and distilled water to maintaining the volume constant. The observed results are depicted graphically in Fig. 1 as absorbance-wavelength reaction profile. Inspection of these results indicates that the absorbance of Pas peak intensity at 270 nm decreases with the reaction time. A new peak appeared at ca. 450 nm, indicating the formation of AgNPs [38]. The intensity of

Table 1
Effects of Pas, Ag^+, CTAB and SDS concentrations of the stability and morphology of AgNPs.

[Pas] (%)	[Ag^+] (mM)	CTAB/SDS	Observations
10	1.0	0.0	Pale yellow, λ_{max} = 438 nm, stable one week
20	1.0	0.0	Pale yellow, λ_{max} = 443 nm, stable one week
30	1.0	0.0	yellow, λ_{max} = 440 nm, stable one week
40	1.0	0.0	Orange, λ_{max} = 454 nm, stable one week
50	1.0	0.0	Orange, λ_{max} = 465 nm, stable one week
60	1.0	0.0	Light orange, λ_{max} = 476 nm, unstable
70	1.0	0.0	Light yellow, λ_{max} = 464 nm, unstable
40	3.0	0.0	Orange, broad shoulder, stable for one week
40	4.0	0.0	Orange, broad shoulder, stable one week
10	0.0	0.4 mM (CTAB)	White turbidity
10	0.0	1.0	White turbidity
10	1.0	4.0 mM (SDS)	Orange, λ_{max} = 420 nm, stable one week
10	1.0	8.0	Orange, λ_{max} = 420 nm, stable one week
10	1.0	12.0	Orange, λ_{max} = 420 nm, stable one week
10	1.0	16.0	Orange, λ_{max} = 420 nm, stable one week
10	1.0	24	Yellow, No SPR band, stable one week
10	1.0	32.0	Yellow, No SPR band, stable one week
10	1.0	40.0	Yellow, No SPR band, stable one week
10	1.0	48.0	Yellow, No SPR band, stable one week

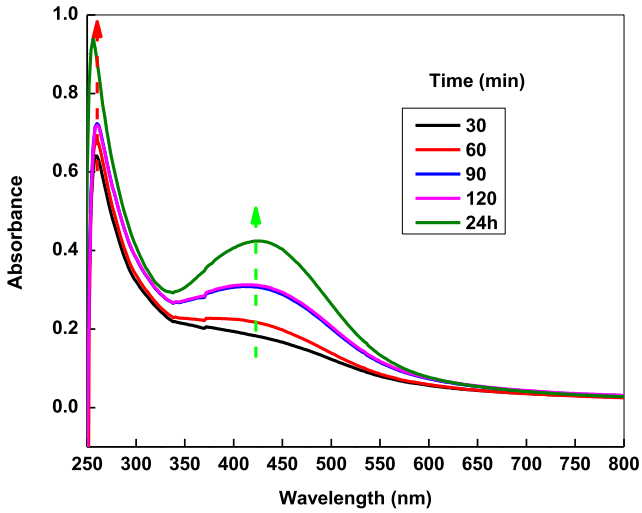

Fig. 4. Effects of SDS on the time-resolved UV–visible spectra of AgNPs formation at 25 °C. Reaction conditions: [Pas] = 10%, [$AgNO_3$] = 1.0 mM, [SDS] = 4.0 (A), 16.0 (B), and 20.0 (C).

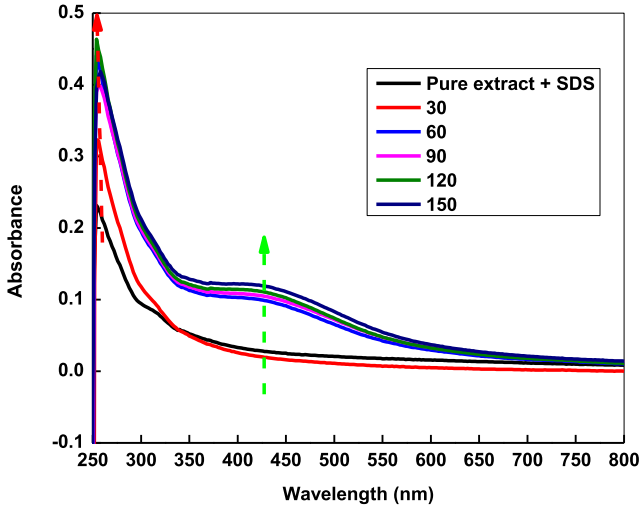

Fig. 4 (*continued*)

SPR peak was remained constant with increasing reaction time from 30 to 180 min at a fixed Pas concentration (Fig. 1A and supporting information Fig.S1). For the comparison, the time-resolved UV–visible spectra of AgNPs were summarized in Fig. 1B for different Pas concentrations. Position of SPR band was red shifted from 438 nm to 475 nm (total = 37 nm shift) with increasing concentration of Pas from 10 to 70% (Fig. 2). The appearance of new SPR peak at 450 nm, intensity decreases at 270 nm and λ_{max} of peak clearly indicates the reduction of Ag^+ ions into Ag^0 by –OH group of Pas and leads to the formation of stable AgNPs. An optical image of resulting AgNPs also shows that the color of silver sols depends on the concentration of Pas. These observations can be rationalized due to the reducing and capping nature of PAs.

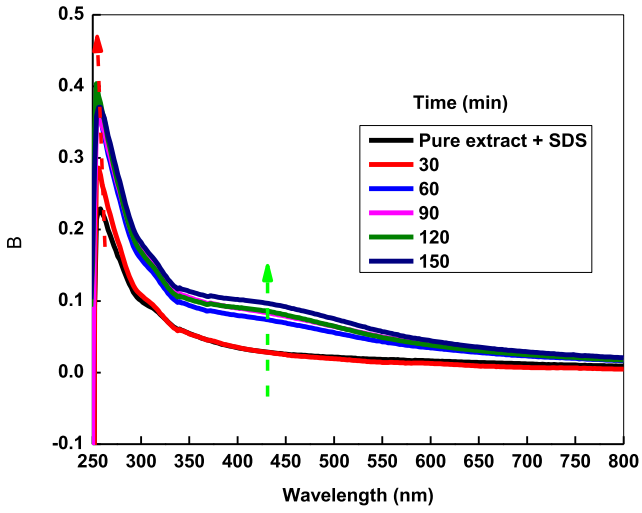

Fig. 4 (*continued*)

In the second set of kinetic experiments, the $AgNO_3$ concentration was varied from 1.0 mM to 4.0 mM at constant concentration of Pas (50 %) and UV–visible spectra were recorded at different time intervals. The peak intensity remain constant with increasing reaction time at [$AgNO_3$ = 1.0 mM (Fig. 3A) and sharp SPR band appeared at 450 nm, indicates that the nucleation was stopped at lower concentration. As the $AgNO_3$ concentration increases, the SPR intensity increases with time and broad shoulder were formed instead of SPR band (Fig. 3 B and C). Thus Ag^+ ions also controlled the nucleation as well as growth processes. Finally, the as prepared AgNPs was stabilized by Pas due to the adsorption of PAs onto the surface of NPs through electrostatic and van der Walls forces between the positive surfaces of NPs and —OH groups lone pairs of electrons (Scheme 2).

3.3. Mechanism of AgNPs formation and capping of Pas

Henglein used photochemical radiation technique to the reduction of Ag^+ ions and reported that the various colloidal silver species were formed in an aqueous solution [39]. They also suggested the formation of Ag_4^{2+} as a stable colloidal silver species in absence of any polymeric stabilizer. The reduction potential of Ag^+/Ag^0 is 0.799 V, which can easily, takes the electron from the available reducing agent and stable colloidal silver was formed.

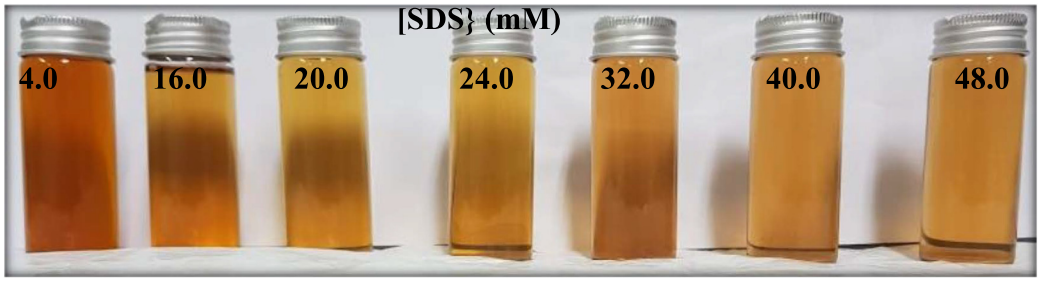

Scheme 5. Effect of SDS on the SPR intensity of AgNPs.

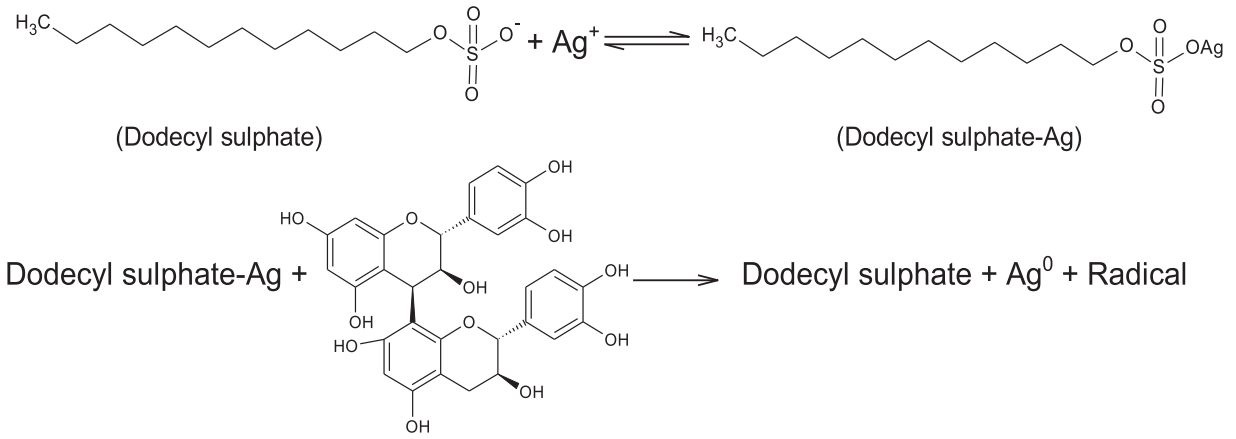

Scheme 6. Effect of SDS on the reduction of Ag^+ by Pas.

In the present study, the appearance of stable colored AgNPs indicates that the Ag^+ gains the electron from the –OH groups of Pas and leads to the formation of AgNPs (Scheme 3).

In Scheme 3, first step represents the reduction of Ag^+ into Ag^0 by –OH of PAs (one-step oxidation–reduction mechanism as a rate determining step. The resulting corresponding radical loss the electron and converted into stable oxidation product of PAs. The Ag^0 was formed complex with Ag^+ very rapidly (Ag_2^+), which undergoes dimerization and Ag_4^{2+} was generated as the stable colloidal silver. The Ag_4^{2+} was stabilized for ca. one week by the adsorption of PAs molecules (Scheme 2). In support of the proposed mechanism, the 5.0 ml of acrylonitrile (CH_2 = CHCN) was added in three different reaction mixtures having only Ag^+, Pas and Ag^+ + Pas. The white precipitate was appeared in the solution of Ag^+ + Pas after some time. Such type of precipitate was not formed with only Ag^+ and Pas solutions. The appearance of precipitate indicates the generation of in-situ free radical during the redox reaction of Ag^+ + Pas [40].

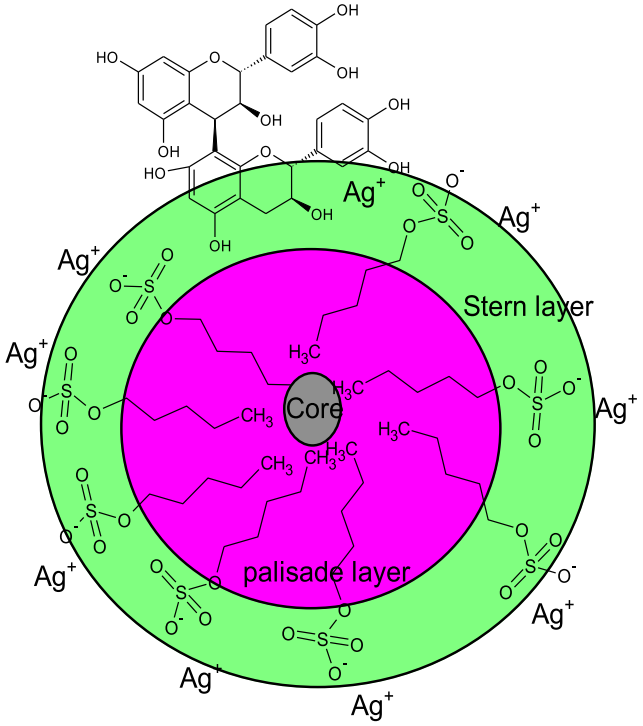

Scheme 7. Probable schematic role of SDS during the AgNPs formation.

3.4. Effect of CTAB and SDS on nucleation and growth

It is well known that the surfactants formed aggregates (micelles) at a specific concentration, solubilizes the hydrophilic and hydrophobic compounds into its small volume and governed the morphology of NPs. CTAB acted as excellent stabilizer and its presence is essential for the preparation of Nps having different morphology [16,17]. Therefore, CTAB was used as a stabilizer in the present study. Preliminary observations shows that the aqueous solution of CTAB (0.4 mM) became white turbid after the addition of 10% Pas solution (Scheme 4).

The turbidity increases with increasing the CTAB concentration (Table 1). Due to the solubility problem with CTAB, we use SDS as capping agent for the synthesis of AgNPs. A series of experiments were carried out with different concentrations of SDS (from 4.0 to 48.0 mM) at fixed Pas concentration. No white precipitate and/or turbidity were formed with SDS and Pas. Time-resolved UV–visible spectra of AgNPs clearly show that the SDS changed the entire shape of SPR band. At lower SDS (=4.0 mM), the resulting silver sol show SPR band at ca. 420 nm after 120 min (Fig. 4A). As the SDS concentration increases, a broad shoulder was formed instead of sharp band in the entire visible region (Fig. 4B and 4C). No significant SPR band and intensity was appeared at higher SDS concentrations ranging from 16.0 mM to 48.0 mM. These results are summarized in supporting information (Fig. S2A, S2B,

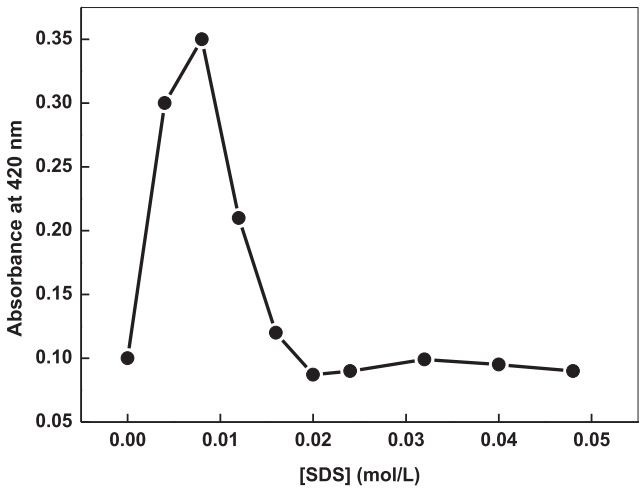

Fig. 5. Effects of SDS on the SPR intensity of AgNPs after 150 min of reaction time at 25 °C. Reaction conditions: [Pas] = 10% and [$AgNO_3$] = 1.0 mM.

S2C and S2D) for different SDS concentrations. Interestingly, the peak intensity of PAs increases at 270 nm with increasing the reaction time, as indicated by red arrow in Fig. 4. Optical images of SDS capped AgNPs were also the color intensity decreases with increasing SDS concentrations (Scheme 5). The resulting silver sols were stable for ca. one week for all SDS and no agglomeration and precipitation was observed.

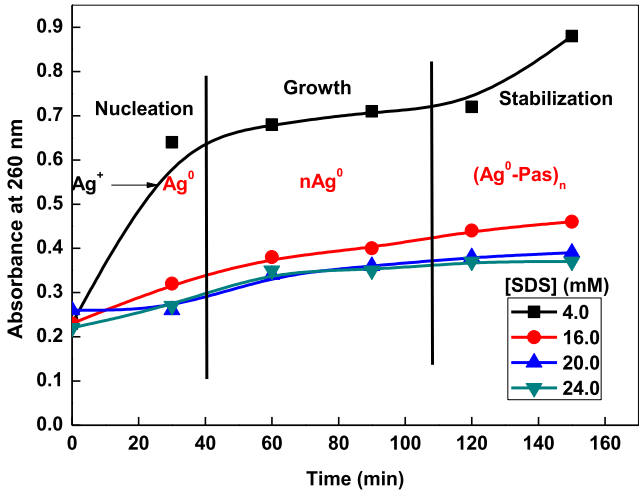

Fig. 5 (*continued*)

Table 2
Effects of Pas, Ag^+, and SDS concentrations on the nucleation-growth kinetics of AgNPs Formation.

[Pas] (%)	[Ag^+] (mM)	SDS (mM)	$10^4 k_{obs}$ (s^{-1})
10	1.0	0.0	2.4
20	1.0	0.0	2.8
30	1.0	0.0	3.4
40	1.0	0.0	3.9
50	1.0	0.0	4.4
60	1.0	0.0	4.9
70	1.0	0.0	3.0
10	1.0	8.0	5.4
10	1.0	8.0	5.2
10	1.0	8.0	5.4
10	1.0	8.0	5.3
10	1.0	4.0	2.8
10	1.0	6.0	3.5
10	1.0	10.0	5.4
10	1.0	12.0	5.8
10	1.0	16.0	5.4
10	1.0	20.0	4.7

In presence of SDS, the Scheme 3 mechanism was modified as Scheme 6.

Ionic surfactant acted as an electrolyte in aqueous solution and formed corresponding ions at lower surfactant concentration [41,42]. They formed various aggregates such as monomer-, dimmer, trimmer, etc. at lower concentration. Micelles were formed at critical micellar concentration. In case of SDS, Ag^+ interacts with ionized dodecyl sulphate and dodecyl sulphate-Ag complex was formed, which takes the electrons from the Pas. Finally SDS capped AgNPs was formed under the experimental conditions. The reduction potential of Ag^+/Ag^0 was reduced to some extent after the complex formation (dodecyl sulphate-Ag) [43], which delayed the electron transfer between the reductant and oxidant. As a result, nucleation and growth rate of AgNPs would be slow for the SDS assisted synthesis of AgNPs. Comparison of Figs. 1 and 4 clearly indicates that the SPR intensity of AgNPs is different for the same reaction time. Three factors, namely, complexation, decrease in reduction potential, and solubilization of reactants (Ag^+ and PAs) occurred simultaneously in presence of SDS (Scheme 7).

Fig. 5A indicates that the SPR intensity of AgNPs increases with SDS concentrations and reaches a maxima at ca. 0.01 mol/L. SPR intensity decreases from 0.35 to 0.09 with SDS ranging from 0.01 to 0.02 mol/L and became constant at higher concentration (≥0.02 mol/L). Reaction-time profiles also shows the nucleation and growth kinetics strongly depends on the SDS concentrations (Fig. 5B). The values of pseudo-first-order rate constants were calculated with the following kinetic equation for the SDS-capped AgNPs formation [44].

$$k_{obs} = \frac{1}{t} \ln \frac{A_\alpha - A_0}{A_\alpha - A_t} \quad (1)$$

where A is the absorbance of AgNPs at completion of the reaction (A_α), initial time (A_0), and different time intervals (A_t). Table 2 shows that the k_{obs} increases with increasing SDS concentrations (from 4.0 to 10.0 mM) and decreases at higher [SDS] (≥12.0 mM). Pre-, Post-, and dilution- micellar effect was observed in presence of SDS [44,45]. The micellar pseudo phase Menger and Portnoy model [46], modified by Bunton et al. [42,45,47] was employed for the explanation of catalytic role of SDS (Scheme 8).

In Scheme 8, k_w and k_m represents the first-order rate constants in aqueous and micellar media, respectively. K_s and K_{PA} are the binding constants of Ag^+ and PAs with the micellized SDS (D_n = [-SDS] – CMC]. Eq.(2) was derived for the bimolecular reaction by considering the mass balance of Ag^+ ions into aqueous and micellar media ($[Ag^+]_T = [Ag^+]_w + [Ag^+]_m$) and Scheme 8.

$$k_\psi = \frac{k'_w[PAs]_T + (K_s k'_m - k'_w)[D_n]M^s_{Ag}}{(1 + K_s[D_n])} \quad (2)$$

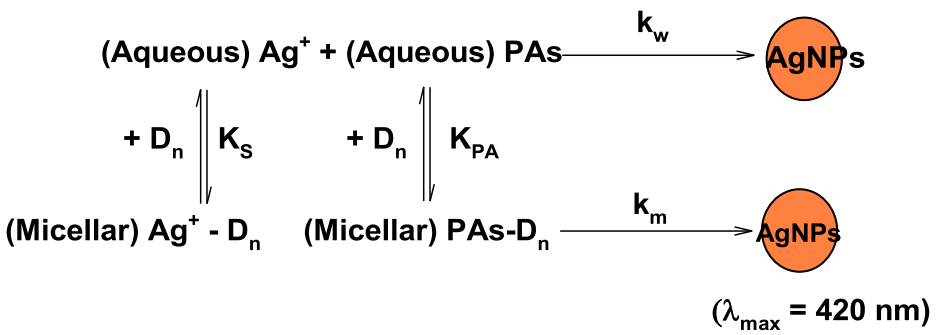

Scheme 8. Role of SDS on the micellization of AgNPs.

where $k_w^{'}$, $k_m^{'}$, and M_{Ag}^{s} are the second-order rate in aqueous, micellar media and the mole ratio of bound Ag^+ with SDS micellar head group, respectively. The values of $k_m^{'}$ = 3.2 × 10^{-3} mol^{-1} dm^3 s^{-1}, K_s = 80 mol^{-1} dm^3 and K_{PA} = 53 mol^{-1} dm^3 were calculated by using a computer programme [24,48,49].

3.5. Morphology and stability of AgNPs

In order to evaluate the shape, size, and the size distribution of as-prepared AgNPs, TEM, SEM and Raman scattering spectrum were recorded. Fig. 6 shows the TEM images of Pas and SDS capped AgNPs. The morphology depend on the concentrations of both Pas and SDS. The particles are spherical, poly-dispersed along with irregular shaped. The truncated triangular nano-plates was also formed. Tiny dots were also appeared in TEM images. Inspection of these images clearly indicates the presence of black spot on the surface of AgNPs, which might be due to the capping action of organic moiety of Pas [50]. SEM images of SDS-capped AgNPs clearly shows that the aggregated and spherical AgNPs were formed and morphology strongly depends on the SDS concentrations (Fig. 7). Surface Enhanced Raman Spectrum (SERS) of SDS-capped AgNPs is given in Fig. 8, which shows the various peak at

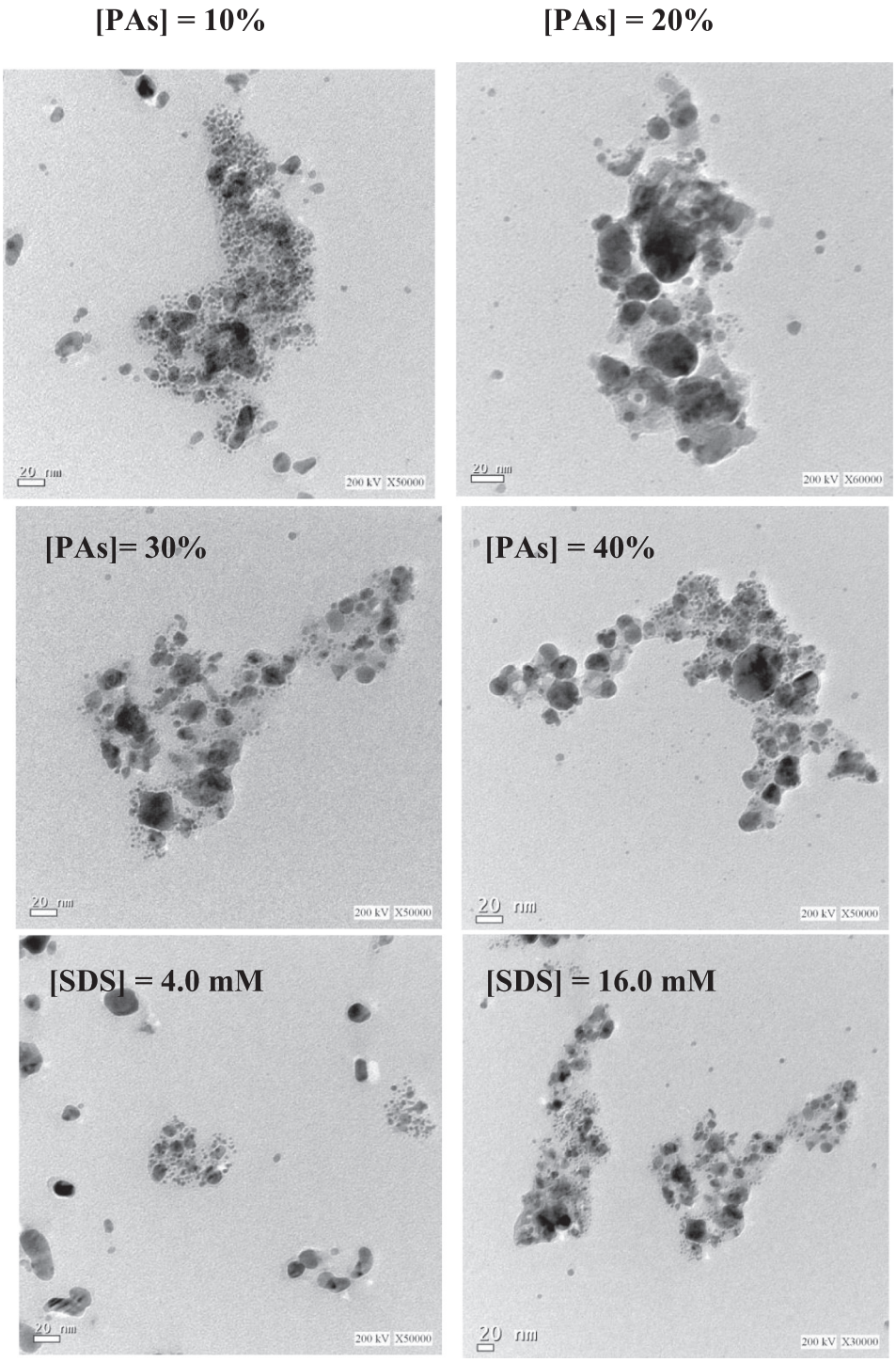

Fig. 6. TEM images of AgNPs for various Pas and SDS concentrations.

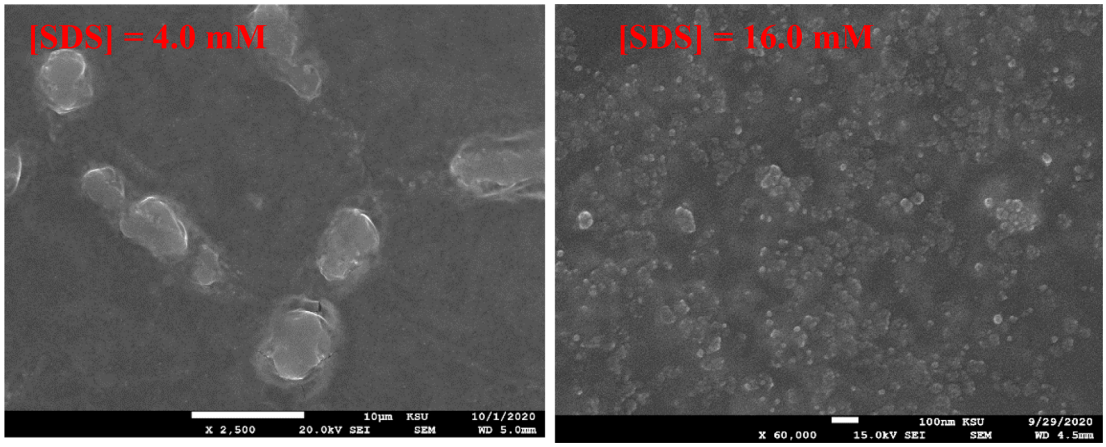

Fig. 7. SEM images of AgNPs for different SDS concentrations.

ca. 647, 924, 1049, 1287, 1357, 1458, 191, 1nd 2938 cm^{-1}. The characteristics part of the SDS SERS were the appearance of peaks in the region from 500 to 900 cm^{-1}, 1050 to 1500 cm^{-1} and 2800 to 2900 cm^{-1} associated to the head group (—OSO_3 and S—O—C vibrational modes), carbon skeleton (C—C stretching, CH_2 twisting and bending modes), and C—H stretching vibration modes, respectively [51–53]. Table 3 indicates that the main characteristic peaks of our SDS-AgNPs are in the close agreement to the reported Raman peaks in the literature for SDS with different complex forming agents [51–53]. In SDS-AgNPs, the polar head group, C—C, CH_2 and C—H peaks were shifted in comparison to pure SDS, which might be due to the strong interaction between them (Table 3). The appearance of major two peaks at ca. 1049 and 1489 cm^{-1} (Fig. 8) with high Raman intensity clearly suggested that the Raman spectrum of surfactant was mainly dominated by the vibrational modes of the hydrocarbon chain [51]. The vibrational peaks of SDS head group (SO_3, S—O—C, and S—O) depends on the nature of ligands.

No aggregation, color changes, and any type of visual turbidity was observed for ca. 6 months, indicating that the SDS-capped AgNPs were stable. Our observations are in good agreement to the results of other investigators regarding the higher stability of SDS-capped AgNPs than that of CTAB [54], citric acid [55] and PVP [56]. This can be attributed to the formation of complex and/or double layer of SDS onto the surface of AgNPs. In order to see insight into the stability of AgNPs, zeta potential of SDS-AgNPs and extract-AgNPs were also estimated by using the following equation (Smoluchowski relation; Eq. (3)) [57].

$$\zeta = \frac{4\pi\eta}{D} \times Electrophoretic\ mobility \tag{3}$$

where, ζ = zeta potential, π = 3.14, η = viscosity of the solvent (water), and D = dielectric constant of water. Fig. 9 shows the values of zeta potential as a function of days, which was found to be constant (ca. −24.8 mV) with increasing the days, indicating the SDS-AgNPs are stable at room temperature [58]. For extract-AgNPs, zeta potential decreases with time from −9.0 to 4.0, indicating SDS is a better capping agent in comparison to the plant extract.

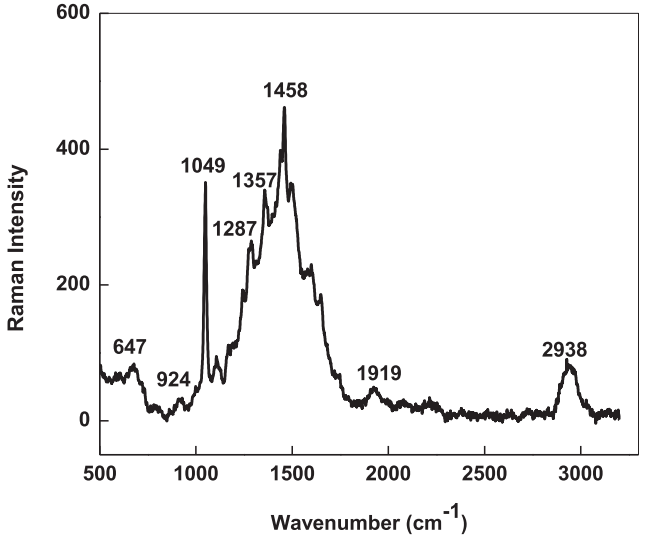

Fig. 8. Raman spectra of SDS-capped AgNPs.

Table 3
Characteristics SERS peaks (in cm^{-1}) of SDS and SDS-Ag NPs.

SDS	SO_3	S—O—C	S—O	C—C	CH_2	C—H	Reference
Solid	635	841	1000	1065	1458	2961	54
Solid	600	995	1063	1132	1468	2935	56
Solid	685	920	1070	1130	1429	2965	55
SDS-Ag	647	924	1049	1287	1458	2938	Present work

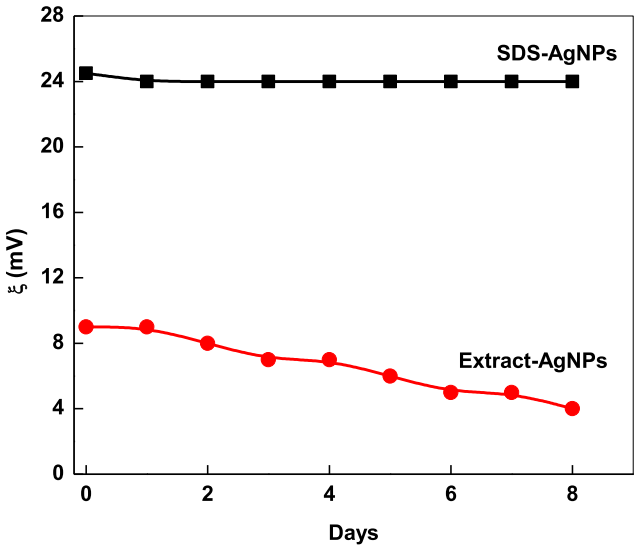

Fig. 9. Zeta potential of Pas-AgNPs and SDS-AgNPs as a function of time. Particle charge was negative in both cases.

4. Conclusion

We described the role of ionic head groups of anionic SDS and cationic CTAB on the nucleation and growth of AgNPs. The SDS-capped AgNPs was stable at room temperature. SPR intensity and peak position depends on the concentrations of SDS and Pas. The negative head group of SDS interacts with Ag^+ ions and formed a complex. Due to the formation of white precipitate, CTAB is not a suitable stabilizer in the present redox system (Pas + Ag^+). Ag^+ ions solubilized into the anionic micelles of SDS. The reduction of coordinated silver ions by –OH group of PAs occurred in the Stern-layer. Thus we may state confidently that the presence of a suitable stabilizer is essential to the fabrication of prefect transparent and stable AgNPs. The presented approach appears to be a successful methodology to the evaluation of capping action of stabilizer that govern the morphology of transition metal NPs and Raman spectroscopy can be used to integrate the role of surfactant.

Declaration of Competing Interest

The authors declare that they have no known competing financial interests or personal relationships that could have appeared to influence the work reported in this paper.

Appendix A. Supplementary material

Supplementary data to this article can be found online at https://doi.org/10.1016/j.molliq.2021.117309.

References

[1] M.S. Bakshi, Impact of nanomaterials on terrestrial flora and aquatic life: mechanistic aspects in vivo, Environ. Res. 182 (2020) 109099.
[2] M.S. Bakshi, Nanotoxicity in systemic circulation and wound healing, Chem. Res. Toxicol. 30 (2017) 1253–1272.
[3] M.S. Bakshi, Colloidal micelles of block copolymers as nanoreactors, templates for gold nanoparticles, and vehicles for biomedical applications, Adv. Colloid Interf. Sci. 213 (2014) 1–20.
[4] M.S. Bakshi, Nanoshape control tendency of phospholipids and proteins: Protein- nanoparticles composites, seeding, self-aggregation, and their applications in bio-nanotechnology and nanotoxicology, J. Phys. Chem. C 115 (2011) 13947–13960.
[5] S.A. Kosa, Z. Zaheer, Betanin assisted synthesis of betanin@silver nanoparticles and their enhanced adsorption and biological activities, Food Chem. 298 (2019) 125014.
[6] Z. Zaheer, Eco-friendly walnut shell powder based facile fabrication of biogenic Ag-nanodisks, and their interaction with bovine serum albumin, J. Photochem. Photobiol. B: Biol. 193 (2019) 8–17.
[7] S.A. Kosa, Zoya Zaheer Sodium dodecyl sulfate assisted synthesis, optical properties and catalytic activities of silver/manganese dioxide nanocomposites, J. Mole. Liquids 258 (2018) 310–318.
[8] M.S. Bakshi, How surfactants control crystal growth of nanomaterials, Cryst. Growth Des. 16 (2) (2016) 1104–1133.
[9] M. Verma, K. Singh, M.S. Bakshi, Surface active magnetic iron oxide nanoparticles for extracting metal nanoparticles across an aqueous–organic interface, J. Mater. Chem. C 7 (34) (2019) 10623–10634.
[10] A. Mahal, L. Tandon, P. Khullar, G.K. Ahluwalia, M.S. Bakshi, pH responsive bioactive lead sulfide nanomaterials: protein induced morphology control, bioapplicability, and bioextraction of nanomaterials, ACS Sustain. Chem. Eng. 5 (1) (2017) 119–132.
[11] V.K. Sharma, R.A. Yngard, Y. Lin, Silver nanoparticles: green synthesis and their antimicrobial activities, Adv. Colloid Interf. Sci.nce 145 (2009) 83–96.
[12] P. Raveendran, J. Fu, S.L. Wallen, J. Am. Chem. Soc. 125 (2003) 13940–13941.
[13] Z. Khan, Chitosan capped Au@Pd@Ag trimetallic nanoparticles: synthesis, stability, capping action and adsorbing activities, Int J. Biol. Macromole. 153 (2020) 545–560.
[14] S. Sengupta, D. Eavarone, I. Capila, G.L. Zhao, N. Watson, T. Kiziltepe, R. Sasisekharanet, Nature 436 (2005) 568–572.
[15] I. Lisiecki, F. Billoudet, M.P. Pileni, Control of the shape and the size of copper metallic particles, J. Phys. Chem. 100 (1996) 4160–4166.
[16] S. Chen, Z.L. Wang, J. Ballato, S.H. Foulger, D.L. Carroll, Monopod, Bipod, tripod, and tetrapod gold nanocrystals, J. Am. Chem. Soc. 125 (52) (2003) 16186–16187.
[17] T.K. Sau, C.J. Murphy, Room temperature, high-yield synthesis of multiple shapes of gold nanoparticles in aqueous solution, J. Am. Chem. Soc. 126 (28) (2004) 8648–8649.
[18] E. Hao, R.C. Bailey, G.C. Schatz, J.T. Hupp, S.Y. Li, Synthesis and optical properties of "branched" gold nanocrystals, Nano Lett. 4 (2004) 327–330.
[19] C.-H. Kuo, M.H. Huang, Synthesis of branched gold nanocrystals by a seeding growth approach, Langmuir 21 (5) (2005) 2012–2016.
[20] O.M. Bakr, B.H. Wunsch, F. Stellacci, High-yield synthesis of multi-branched urchin-like gold nanoparticles, Chem. Mater. 18 (14) (2006) 3297–3301.
[21] J. Xiao, L. Qi, Surfactant-assisted, shape-controlled synthesis of gold nanocrystals, Nanoscale 3 (4) (2011) 1383, https://doi.org/10.1039/c0nr00814a.
[22] O.M. Khabeeri, S.A. Al-Thabaiti, Z. Khan, Effects of ionic surfactants on the nucleation and growth of cyanidin 3,5-di-O-glucoside capped zerovalent iron nanoparticles, Coll. Interf. Sci. Comm. 37 (2020) 100272, https://doi.org/10.1016/j.colcom.2020.100272.
[23] M. Kalkan Erdoğan, Preparation and stabilization of Ag nanoparticles with N-vinyl-2- pyrrolidone grafted-poly(vinyl alcohol) in an organic medium and investigation of their usability in the catalytic dye decolorization, Coll. Interf. Sci. Comm. 34 (2020) 100222, https://doi.org/10.1016/j.colcom.2019.100222.
[24] H.U. Gali-Muhtasib, S.Z. Yamout, M.M. Sidani, Tannins protect against skin tumor promotion induced by ultraviolet-B radiation in hairless mice, Nutr. Cancer 37 (1) (2000) 73–77.
[25] W. Hümmer, P. Schreier, Analysis of proanthocyanidins, Mol. Nutr. Food Res. 52 (12) (2008) 1381–1398.
[26] G. Dinelli, A. Segura-Carretero, R. Di Silvestro, I. Marotti, D. Arráez-Román, S. Benedettelli, L. Ghiselli, A. Fernadez-Gutierrez, Profiles of phenolic compounds in modern and old common wheat varieties determined by liquid chromatography coupled with time-of-flight mass spectrometry, J. Chromatogr. A 1218 (42) (2011) 7670–7681.
[27] J. Valls, S. Millán, M.P. Martí, E. Borràs, L. Arola, Advanced separation methods of food anthocyanins, isoflavones and flavanols, J. Chromatogr. A 1216 (43) (2009) 7143–7172.
[28] H. Jouad, M. Maghrani, M. Eddouks, Hypoglycaemic effect of Rubus fructicosis L. and Globularia alypum L. in normal and streptozotocin-induced diabetic rats, J. Ethnopharmac. 81 (3) (2002) 351–356.
[29] M.A. Marquina, G.M. Corao, L. Araujo, D. Buitrago, M. Sosa, Hyaluronidase inhibitory activity from the polyphenols in the fruit of blackberry (Rubus fruticosus B.), Fitoterapia 73 (7-8) (2002) 727–729.
[30] C.-F. Zhao, D.J. Lei, G.H. Song, H. Zhang, H. Xu, L.-J. Yu, Characterisation of water-soluble proanthocyanidins of Pyracantha fortuneana fruit and their improvement in cell bioavailable antioxidant activity of quercetin, Food Chem. 169 (2015) 484–491.
[31] M. Jerez, S. Tourino, J. Sineiro, J.L. Torres, M.J. Nunez, Procyanidins from pine bark: relationships between structure, composition and antiradical activity, Food Chem. 104 (2007) 518–527.
[32] V.S. Chedea, C. Echim, C. Braicu, M. Andjelkovic, R. Verhe, C. Socaciu, Composition in polyphenols and stability of the aqueous grape seed extract from the Romanian variety " Merlot recas", J. Food Biochem. 35 (2011) 92–108.
[33] X.-X. Chen, H.-L. Feng, Y.-M. Ding, W.-M. Chai, Z.-H. Xiang, Y. Shi, Q.-X. Chen, Structure characterization of proanthocyanidins from caryota ochlandra Hance and their aioactivities, Food Chem. 155 (2014) 1–8.
[34] L.-Z. Lin, J.M. Harnly, Quantitation of flavanols, proanthocyanidins, isoflavones, flavanones, dihydrochalcones, stilbenes, benzoic acid derivatives using ultraviolet absorbance after identification by liquid chromatography–mass spectrometry, J. Agric. Food Chem. 60 (2012) 5832–5840.
[35] L.H. Yao, Y.M. Jiang, J. Shi, F.A. Tomás-Barberán, N. Datta, R. Singanusong, S.S. Chen, Flavonoids in food and their health benefits, Plant Foods Human Nutr. 59 (2004) 113–122.
[36] C.S. Ku, S.P. Mun, Characterization of proanthocyanidin in hot water extract isolated from *Pinusradiata* bark, Wood Sci. Technol. 41 (3) (2007) 235–247.
[37] E. Revilla, M. Bourzeix, E. Alonso, Analysis of catechins and proanthocyanidins in grape seeds by HPLC with photodiode array detection, Chromalographia 31 (9-10) (1991) 465–468.
[38] A.B. Albeladi, S.A. Al-Thabaiti, Z. Khan, Effect of CTAB on the surface resonance plasmon intensity of silver nanoparticles: stability and oxidative dissolution, J. Mol. Liq. 302 (2020).
[39] A. Henglein, Physicochemical properties of smallmetal particles in solution: "microelectrode" reactions, chemisorption, composite metal particles, and the atom to metal transition, J. Phys. Chem. 97 (1993) 5457–5471.
[40] Z. Khan, S.A. Al-Thabaiti, S. Hussain, Nano scale water soluble self-assembled zerovalent iron: role of stabilizers on their morphology, RSC Adv. 6 (2016) 7267–7278.
[41] F. Rahman, M.Z.A. Rafiquee, Studies on the influence of surfactant on the kinetics of formation of silver nanoparticles by using Croton bonplandianum as green reducing agent, J. Mol. Liq. 258 (2018) 269–274.
[42] C.A. Bunton, L.B. Robinson, Micellar effects upon the reaction of p-nitrophenyl diphenyl phosphate with hydroxide and fluoride ions, J. Org. Chem. 34 (4) (1969) 773–780.
[43] D.V. Goia, E. Matijević, Preparation of monodispersed metal particles, New J. Chem. 22 (11) (1998) 1203–1215.
[44] S.A. Al-Thabaiti, F.M. Al-Nowaiser, A.Y. Obaid, A.O. Al-Youbi, Z. Khan, Formation and characterization of surfactant stabilized silver nanoparticles: a kinetic study, Colloids Surfaces B: Biointerfaces 67 (2) (2008) 230–237.
[45] C.A. Bunton, N. Carrasco, S.K. Huang, C.H. Paik, L.S. Romsted, Reagent distribution and micellar catalysis of carbocation reactions, J. Am. Chem. Soc. 100 (17) (1978) 5420–5425.
[46] F.M. Menger, C.E. Portnoy, Chemistry of reactions proceeding inside molecular aggregates, J. Am. Chem. Soc. 89 (18) (1967) 4698–4703.

[47] C.A. Bunton, The dependence of micellar rate effects upon reaction mechanism, Adv. Colloid Interf. Sci. 123-126 (2006) 333–343.
[48] Kabir-ud -Din, K. Hartani, Z. Khan, Effect of micelles on the oxidation of oxalic acid by chromium(VI) in the presence and absence of mangane se(II), Colloids Surf. A: Physicochem. Eng. Aspect 193 (1-3) (2001) 1–13.
[49] M.A. Malik, Z. Khan, Role of cetyltrimethylammonium bromide (cationic surfactant) on the tryptophan–MnO_4^- reaction, Colloids Surfaces B: Biointerfaces 72 (2) (2009) 253–258.
[50] S.S. Shankar, A. Rai, A. Ahmad, M. Sastry, Rapid synthesis of Au, Ag, and bimetallic Au core-Ag shell nanoparticles using Neem (Azadirachta indica) leaf broth, J. Colloid Interface Sci. 275 (2) (2004) 496–502.
[51] M. Picquart, Vibrational mode behavior of SDS aqueous solutions studied by Raman Scattering, J. Phys. Chem. 90 (1986) 243–250.
[52] A.R. Paschoal, A.P. Ayala, R.C.F. Pinto, C.W.A. Paschoal, A.A. Tanaka, J.S. Boaventura Filho, N.M. Jose, About the SDS inclusion in PDMS/TEOS ORMOSIL: a vibrational spectroscopy and confocal Raman scattering study, J. Raman Spectrosc. 42 (2011) 1601–1605.
[53] G. Cazzolli, S. Caponi, A. Defant, C.M.C. Gambi, S. Marchetti, M. Mattarelli, M. Montagna, B. Rossi, F. Rossi, G. Viliani, Aggregation processes in micellar solutions: a Raman study, J. Raman Spectrosc. 43 (12) (2012) 1877–1883.
[54] Y.-H. Chen, C.-S. Yeh, Laser ablation method: use of surfactants to form the dispersed Ag nanoparticles, Colloids Surf. A. Physicochem. Eng. Asp. 197 (1-3) (2002) 133–139.
[55] F.K. Liu, F.H. Ko, P.W. Huang, C.H. Wu, T.C. Chu, Studying the size/shape separation and optical properties of silver nanoparticles by capillary electrophoresis, J. Chromatogr. A 1062 (2005) 139–145.
[56] K.H. Cho, J.E. Park, T. Osaka, S.G. Park, The study of antimicrobial activity and preservative effects of nanosilver ingredient, Electrochim. Acta 51 (2005) 956–960.
[57] A.J. Kora, R. Manjusha, J. Arunachalam, Superior bactericidal activity of SDS capped silver nanoparticles: synthesis and characterization, Mater. Sci. Eng., C 29 (7) (2009) 2104–2109.
[58] M.F. Melendrez, G. Cardenas, J. Arbiol, Synthesis and characterization of gallium colloidal nanoparticles, J. Colloid Interface Sci. 346 (2010) 279–287.